Journal Article

Thermal-vibration investigation of a functionally graded doubly-curved sandwich structure using three dimensional spectral-Chebyshev approach

Anamagh, M.R. and Day, R.J.

Thermal-vibration investigation of a functionally graded doubly-curved sandwich structure using three dimensional spectral-Chebyshev approach

Mirmeysam Rafie Anamagh[a,*], Richard J. Day[a]

[a] *Faculty of Arts, Computing and Engineering, Wrexham University, Wrexham, UK*

Abstract

This research presents a novel three-dimensional numerical approach to investigate the dynamic behavior of doubly-curved sandwich structures reinforced with functionally graded material face-sheets. A three-dimensional spectral Chebyshev method is developed to solve the resulting integral boundary value problem, which incorporates the effects of temperature variation across the sandwich structure. To facilitate the numerical implementation, a mapping technique is employed to transform the complex geometry into a simplified computational domain using appropriate transformation equations. The proposed spectral Chebyshev approach is validated by computing the natural frequencies of selected sandwich configurations and comparing them with results available in the literature. In addition to the validation study, extensive parametric analyses are performed to assess the influence of various material parameters (such as the power-law index of the FGM) and geometric parameters (including curvature magnitude and length ratios) on the natural frequencies of the structure. Furthermore, the effects of different thermal gradients across the thickness are systematically examined under various boundary conditions. The findings highlight the critical role of thermal variation and boundary support conditions in altering the dynamic response of sandwich structures. This study provides valuable insights for the design and optimization of advanced composite structures subjected to thermo-mechanical environments.

Keywords: composites; sandwich-structured composite; functionally graded; spectral Chebyshev; thermal.

1. Introduction

The quest for advanced structural materials capable of withstanding extreme mechanical and thermal environments has been a driving force in engineering innovation for decades. In 1972, Shen and Bever [1] first introduced the concept of Functionally Graded Materials (FGMs) as a novel solution to overcome the limitations of traditional composites and polymers. Initially developed to improve bonding strength and reduce thermal stresses in coating applications, FGMs have since evolved into one of the most promising material systems for high-performance structures. A landmark in the practical use of FGMs occurred in 1984, when Japan's National Aerospace Laboratories implemented graded materials in aerospace applications, specifically for fuselage base shells and nosecone components of a spaceplane. These early implementations highlighted the unmatched ability of FGMs to manage high thermal gradients, resist delamination, and reduce stress concentrations, challenges that often compromise the integrity of conventional layered composites.

FGMs are characterized by their continuous variation in material composition, typically transitioning from ceramic to metal across the thickness of a structure [2]. This gradation endows FGMs with a unique combination of desirable properties, high-temperature resistance from ceramics and toughness and thermal conductivity from metals, while avoiding the stress discontinuities that occur in traditional composites with discrete interfaces [3]. Depending on the phase distribution, FGMs are generally classified into continuously and stepwise graded types. Additionally, they can be categorized into thin FGMs, used primarily in surface coatings via processes such as PVD, SHS, and CVD, and bulk FGMs, manufactured through powder metallurgy, centrifugal casting, and additive techniques [4–6]. These developments have led to widespread applications in aerospace, automotive, energy, and biomedical engineering.

*E-mail: meysam.anamagh@wrexham.ac.uk
[1]Phone: +44-7982-365458

In aerospace, ceramic-metal FGMs serve as thermal barriers, insulating combustion chambers, rocket nozzles, and engine parts against intense thermal fluxes [7]. In medicine, graded biomaterials such as hydroxyapatite-titanium composites have revolutionized implant design, offering superior biocompatibility and mechanical performance for joint replacements and dental restorations [8–10].

As FGMs gained popularity, researchers turned their attention to the complex thermo-mechanical behaviors of these materials, especially in structural elements like plates and shells. Smooth gradation in material properties has proven critical in mitigating issues such as delamination, interfacial cracking, and thermal mismatch [11]. Over the years, extensive theoretical and computational studies have explored the vibration, stress, and buckling responses of FGM structures under mere mechanical load [12–14] or combined with thermal loads [15–17]. Numerous studies have been conducted from various perspectives to analyze the static and dynamic behavior of functionally graded material (FGM) structures. These include static [18, 19], buckling [20, 21], post-buckling [22], thermo-mechanical [23], electro-mechanical [24], thermo-electrical [25–27], pressure [28–30], and stability [31–33] analysis. From reviewing the literature, it is evident that the mentioned studies focus primarily on either single-layer FGM structures or simple sandwich structures without curvature or complexity. This highlights a gap in the research, indicating the need for further analysis of FGM structures in more practical applications, such as curved and complex sandwich configurations.

To conduct the aforementioned analysis, a wide range of analytical and numerical approaches has been employed, spanning from classical plate theory, first-order shear deformation theory (FSDT) [34–36], higher-order shear deformation theories (HSDT) [37, 38], Zig-Zag theory [39] and refined shear deformation theories [40, 41], as well as advanced three-dimensional elasticity models. Thai and Kim [42] and Wu and Liu [43] have provided comprehensive reviews on the evolution of modeling techniques, emphasizing the growing importance of semi-analytical methods such as the finite layer method, state-space approaches, and the sampling surface method for layered and FGM sandwich structures. All the aforementioned theories can be critiqued from two perspectives. Firstly, some theories fail to accurately predict structural behavior due to inherent simplifications. Secondly, when modeling thick structures, a significant computational effort is required, as numerous correction parameters must be introduced to improve accuracy. Therefore, three-dimensional modeling appears to be a suitable and effective choice for analyzing thick structures, especially sandwich configurations, where the constituent layers often consist of distinctly different materials.

On the other hand, extensive research has been conducted to solve the equations of motion derived from the aforementioned modeling theories for functionally graded material (FGM) structures using various numerical techniques. These methods include the radial point interpolation mesh-free method [44], generalized differential quadrature (GDQ) [45, 46], isogeometric analysis [47, 48], meshless local Petrov–Galerkin (MLPG) method [49], finite point multiquadric method [50], differential transformation method (DTM) [51], harmonic differential quadrature (HDQ) [52], and the Chebyshev–Ritz method [53]. Although these approaches can accurately solve the equations of motion, they are often associated with certain drawbacks, such as complex integration over local subdomains, sensitivity to the selection of appropriate basis functions for various boundary conditions, and high computational cost. Among these techniques, the finite element method (FEM) remains the most widely used approach in both academic and industrial settings. Numerous studies have utilized FEM to investigate the static and dynamic behavior of FGM structures under diverse loading and boundary conditions [54–56]. However, despite its widespread adoption and commercialization, FEM may become inefficient when dealing with geometrically complex or three-dimensional models, limiting its applicability for design and optimization tasks. To address these challenges, the authors have recently introduced a novel meshless technique termed the spectral Chebyshev approach, which employs Chebyshev polynomials to discretize the governing equations [57]. This method offers an efficient and accurate solution framework and demonstrates significant potential for structural analysis, particularly in design and optimization problems where computational efficiency is critical.

Despite mentioned progress in modeling and solving approaches, the thermal-vibration analysis of doubly-curved functionally graded sandwich structures remains a relatively underexplored domain, particularly with respect to three-dimensional modeling. Most existing models either simplify the geometry or ignore the coupling effects of curvature and material gradation under thermal loading. To address this gap and due to the importance of structural vibration of structures in industrial application [58–60], the present study introduces a three-dimensional spectral-Chebyshev approach as a meshless, highly accurate method for solving the dynamic response of curved sandwich structures with FGM face-sheets exposed to thermal gradients. By leveraging the spectral-Chebyshev formulation and incorporating curvature via domain mapping, this work aims to capture the detailed thermo-mechanical interactions across the structure's thickness. The method also accommodates various boundary conditions and complex temperature profiles, making it a powerful tool for next-generation composite design.

2. Modeling

Figure 1 illustrates the sandwich structure with functionally graded material (FGM) face sheets in a global coordinate system (x–y–z). The displacement vector is defined as $\mathbf{q} = [u, v, w]$ in (x,y,z) directions, respectively. The core layer consists of purely metal material. The temperatures at the bottom and top surfaces are denoted by T_b and T_t, respectively. The curvatures β_1 and β_2 are defined based on the radii of curvature R_1 and R_2 around the x- and y-axes, respectively. Also, h_1, h_2 and h_3 represent the thicknesses of the bottom, core, and top layers, respectively.

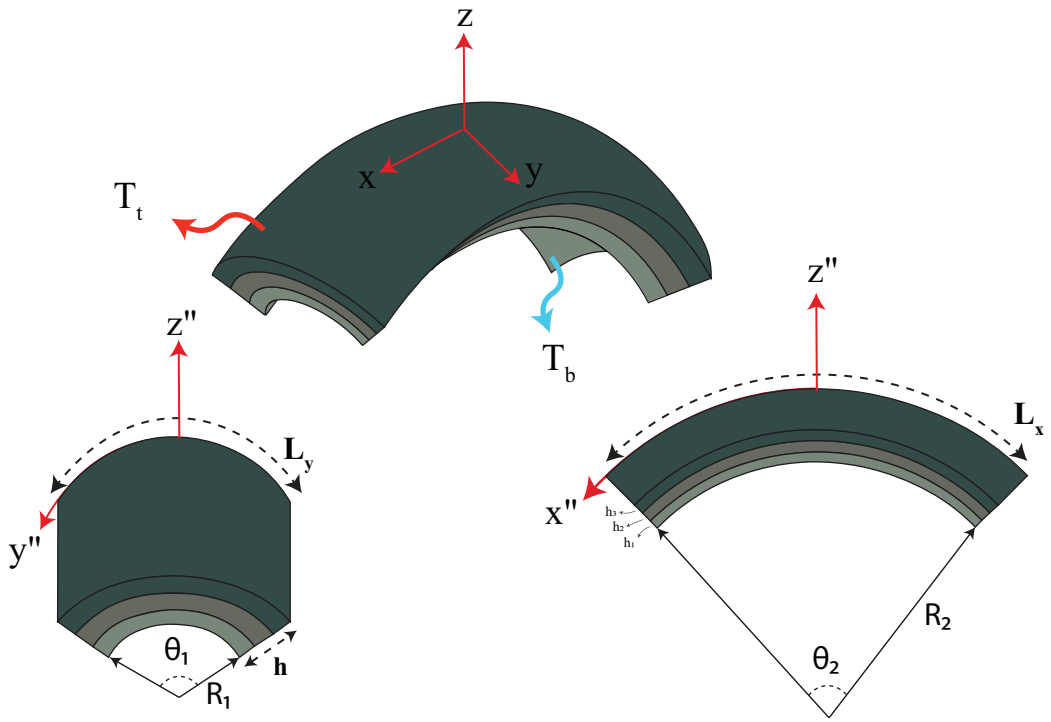

Figure 1: Schematic of a sandwich structure with functionally graded face sheets and an aluminum core in a thermal environment.

For thermally induced free vibration analysis, it is assumed that the structure is initially stress-free at a reference temperature T_0. Upon a temperature rise ΔT, the structure is heated to a steady-state thermal condition and then vibrates in the thermally affected state. This temperature change induces additional strain energy due to thermal stresses constrained by boundary conditions that inhibit in-plane expansion. This initial thermal strain energy is given by [61]:

$$\mathbf{\Pi}_T = \frac{1}{2}\int_V (\bar{\sigma}_{xx}\bar{\epsilon}_{xx} + \bar{\sigma}_{yy}\bar{\epsilon}_{yy})\, dV \tag{1}$$

The thermal stresses $\bar{\sigma}_{xx}$ and $\bar{\sigma}_{yy}$ due to the temperature change can be expressed as:

$$\bar{\sigma}_{ij} = -\frac{C_{ij}(z,T)\alpha(z,T)\Delta T}{1-2\nu(z,T)}\delta_{ij}, \quad i,j = 1,2 \tag{2}$$

Here, C_{ij}, α, ν and δ represent the elastic stiffness components, the thermal expansion coefficient, Poisson's ratio and Kronecker delta, respectively. These parameters vary with both the thickness coordinate z and temperature T due to the FGM nature of the material. It should be noted that, according to the study by Thai et al. [61], in the case of neglecting the out-of-plane components of the thermal stress matrix yields accurate results. The corresponding thermally induced in-plane strains are given by:

$$\bar{\epsilon}_{xx} = \left(\frac{\partial w}{\partial x}\right)^2, \quad \bar{\epsilon}_{yy} = \left(\frac{\partial w}{\partial y}\right)^2 \tag{3}$$

The thermal stiffness matrix resulting from the initial thermal loading can be written as:

$$\mathbf{K}_T = \int_V B_T^{\mathrm{T}} \bar{\sigma}_{ii} B_T \, dV = \int_V \begin{bmatrix} 0 & 0 \\ 0 & 0 \\ \frac{\partial}{\partial x} & \frac{\partial}{\partial y} \end{bmatrix} \begin{bmatrix} -\frac{C_{11}(z,T)\alpha(z,T)\Delta T}{1-2\nu(z,T)} & 0 \\ 0 & -\frac{C_{22}(z,T)\alpha(z,T)\Delta T}{1-2\nu(z,T)} \end{bmatrix} \begin{bmatrix} 0 & 0 & \frac{\partial}{\partial x} \\ 0 & 0 & \frac{\partial}{\partial y} \end{bmatrix} dV \tag{4}$$

In addition to the initial thermal strain energy, the elastic strain energy due to mechanical vibrations is expressed as:

$$\mathbf{\Pi}_e = \frac{1}{2} \int_V \boldsymbol{\epsilon}^{\mathrm{T}} C \boldsymbol{\epsilon} \, dV = \frac{1}{2} \int_V \mathbf{q}^{\mathrm{T}} B^{\mathrm{T}} C B \mathbf{q} \, dV, \quad \mathbf{q} = [u, v, w] \tag{5}$$

where, ϵ is the strain and can be derived for a three dimensional modeling as:

$$\boldsymbol{\epsilon} = \begin{bmatrix} \epsilon_{xx} & \epsilon_{yy} & \epsilon_{zz} & \gamma_{xy} & \gamma_{xz} & \gamma_{yz} \end{bmatrix}^T = \begin{bmatrix} \frac{\partial u}{\partial x} & \frac{\partial v}{\partial y} & \frac{\partial w}{\partial z} & \frac{\partial u}{\partial y} + \frac{\partial v}{\partial x} & \frac{\partial u}{\partial z} + \frac{\partial w}{\partial x} & \frac{\partial v}{\partial z} + \frac{\partial w}{\partial y} \end{bmatrix}^T \tag{6}$$

The constitutive matrix C_{ij} for isotropic materials is defined as:

$$C = \frac{E(z,T)}{1+\nu(z,T)} \begin{bmatrix} \frac{1-\nu(z,T)}{1-2\nu(z,T)} & \frac{\nu(z,T)}{1-2\nu(z,T)} & \frac{\nu(z,T)}{1-2\nu(z,T)} & 0 & 0 & 0 \\ \frac{\nu(z,T)}{1-2\nu(z,T)} & \frac{1-\nu(z,T)}{1-2\nu(z,T)} & \frac{\nu(z,T)}{1-2\nu(z,T)} & 0 & 0 & 0 \\ \frac{\nu(z,T)}{1-2\nu(z,T)} & \frac{\nu(z,T)}{1-2\nu(z,T)} & \frac{1-\nu(z,T)}{1-2\nu(z,T)} & 0 & 0 & 0 \\ 0 & 0 & 0 & \frac{1}{2} & 0 & 0 \\ 0 & 0 & 0 & 0 & \frac{1}{2} & 0 \\ 0 & 0 & 0 & 0 & 0 & \frac{1}{2} \end{bmatrix} \tag{7}$$

Alternatively, using Lamé parameters λ and μ:

$$C = \begin{bmatrix} \lambda+2\mu & \lambda & \lambda & 0 & 0 & 0 \\ \lambda & \lambda+2\mu & \lambda & 0 & 0 & 0 \\ \lambda & \lambda & \lambda+2\mu & 0 & 0 & 0 \\ 0 & 0 & 0 & \mu & 0 & 0 \\ 0 & 0 & 0 & 0 & \mu & 0 \\ 0 & 0 & 0 & 0 & 0 & \mu \end{bmatrix} \tag{8}$$

Here, $E(z,T)$ and $\nu(z,T)$ are the Young's modulus and Poisson's ratio, and λ and μ are the Lamé constants, all of which depend on the coordinate z and temperature T. The strain-displacement derivative matrix B is defined as:

$$B = \begin{bmatrix} \frac{\partial}{\partial x} & 0 & 0 \\ 0 & \frac{\partial}{\partial y} & 0 \\ 0 & 0 & \frac{\partial}{\partial z} \\ \frac{\partial}{\partial y} & \frac{\partial}{\partial x} & 0 \\ \frac{\partial}{\partial z} & 0 & \frac{\partial}{\partial x} \\ 0 & \frac{\partial}{\partial z} & \frac{\partial}{\partial y} \end{bmatrix} \tag{9}$$

Based on Eq. 5, the elastic stiffness matrix is computed as:

$$\mathbf{K}_e = \int_V B^{\mathrm{T}} C B \, dV \tag{10}$$

The kinetic energy of the vibrating system is given by:

$$\mathbf{T} = \frac{1}{2} \int_V \rho(z,T) \left(\dot{u}^T \dot{u} + \dot{v}^T \dot{v} + \dot{w}^T \dot{w} \right) dV \tag{11}$$

Here, $\rho(z,T)$ is the mass density, a function of position and temperature, and $\dot{\mathbf{q}} = [\dot{\mathbf{u}}, \dot{\mathbf{v}}, \dot{\mathbf{w}}]$ represents the velocity vector. The mass matrix can therefore be evaluated as:

$$\mathbf{M} = \int_V \rho(z,T) \, dV \tag{12}$$

Finally, the equation governing the free vibration of the structure is formulated as an eigenvalue problem:

$$\left[(\mathbf{K}_e + \mathbf{K}_T) - \Omega^2 \mathbf{M} \right] \Psi = 0 \tag{13}$$

where Ω denotes the natural frequencies, and Ψ represents the corresponding mode shapes of the structure.

3. Functionally graded material

Functionally graded materials are designed with a focus on structures exposed to high-temperature environments. The material properties of FGMs exhibit consistent variations in response to temperature fluctuations. When FGMs comprise both ceramic and metal components, their material properties can be determined by fitting equations to experimental results [62] as;

$$P_\psi(T) = P_0 \left(\frac{P_{-1}}{T} + 1 + P_1 T + P_2 T^2 + P_3 T^3 \right) \tag{14}$$

In this context, P_ψ can be considered as the elasticity (E), density (ρ), thermal conductivity (k), and thermal expansion coefficient (α) of either the ceramic ($\psi = c$) or the metal ($\psi = m$). Furthermore, the coefficients P_{-1}, P_1, P_2, and P_3 exhibit temperature-dependent parameters. The specific values for these coefficients for stainless steel (metal) and Silicon nitride (ceramic), which constitute the FGM, are detailed in Table 1. As presented in Table 1, the thermal conductivity and density are considered temperature-independent material parameters.

Utilizing the power-law distribution equation, the volumetric fraction of ceramic material throughout the thickness

Table 1: Temperature coefficients of Nickel and Aluminum Oxide in a thermal environment [63].

Material	Properties	P_0	P_{-1}	P_1	P_2	P_3	P @ $T_0 = 300\,\mathrm{K}$
Si_3N_4	E (Pa)	348.43×10^9	0	-3.070×10^{-4}	2.160×10^{-7}	-8.946×10^{-11}	322.2715×10^9
	ν	0.2400	0	0	0	0	0.2400
	α (1/K)	6.8269×10^{-6}	0	1.83×10^{-4}	0	0	7.4746×10^{-6}
	ρ (kg/m^3)	3950	0	0	0	0	3950
	k	9.19	0	0	0	0	9.19
SUS304	E (Pa)	201.04×10^9	0	3.079×10^{-4}	-6.534×10^{-9}	0	207.7877×10^9
	ν	0.3262	0	-2.002×10^{-4}	3.797×10^{-7}	0	0.3178
	α (1/K)	12.330×10^{-6}	0	8.086×10^{-4}	0	0	1.5321×10^{-5}
	ρ (kg/m^3)	8166	0	0	0	0	8166
	k	12.04	0	0	0	0	12.04

can be calculated as follows:

$$V_c = (\frac{1}{2} + \frac{z}{h})^n \tag{15}$$

Here, V_c, h, and n represent the volume fraction of ceramic, the thickness of the structure, and the power-law index, respectively. The material properties of the FGM structure are determined using the rule of mixture.

$$\begin{aligned} &P(z,T) = P_c(T)V_c(z) + P_m(T)V_m(z) \\ &V_m = 1 - V_c \end{aligned} \tag{16}$$

For temperature variation along the thickness of the sandwich structure, three cases are considered: uniform, linear, and nonlinear distributions. It should be noted that the bottom and top surface temperatures are defined as T_b and T_t, respectively. In the case of a uniform field, the temperature along the thickness can be obtained as:

$$T = T_b + \Delta T \tag{17}$$

where ΔT indicates the temperature difference. For the case of linear variation, the temperature field can be expressed as:

$$T(z) = T_b + \Delta T(\frac{z}{h}) \tag{18}$$

where, ΔT is equal to $T_t - T_b$. In the case of nonlinear variation of the temperature, using the heat-conduction rule, the steady-state equation can be derived as follows:

$$-\frac{d}{dz}\Big[k(z)\frac{dT}{dz}\Big] = 0 \tag{19}$$

By substituting Eq. 15 into the heat conduction equation due to the thermal conductivity variation (k) and employing the first seven terms of the polynomial series as described in [64], the thermal variation along the thickness can be determined as follows:

$$\begin{aligned} T(z) = T_m + \frac{\Delta T}{c}\Bigg[&(\frac{z}{h}+\frac{1}{2}) - \frac{k_{cm}}{(n+1)k_m}(\frac{z}{h}+\frac{1}{2})^{(n+1)} \\ &+ \frac{k_{cm}^2}{(2n+1)k_m^2}(\frac{z}{h}+\frac{1}{2})^{(2n+1)} - \frac{k_{cm}^3}{(3n+1)k_m^3}(\frac{z}{h}+\frac{1}{2})^{3n+1} \\ &+ \frac{k_{cm}^4}{(4n+1)k_m^4}(\frac{z}{h}+\frac{1}{2})^{4n+1} - \frac{k_{cm}^5}{(5n+1)k_m^2(\frac{z}{h}+\frac{1}{2})^{5n+1}}\Bigg] \end{aligned} \tag{20}$$

where,

$$c = 1 - \frac{k_{cm}}{(n+1)k_m} + \frac{k_{cm}^2}{(n+1)k_m^2} - \frac{k_{cm}^3}{(n+1)k_m^3}$$

$$+\frac{k_{cm}^4}{(n+1)k_m^4}-\frac{k_{cm}^5}{(n+1)k_m^5} \tag{21}$$

$$k_{cm}=k_c-k_m, \Delta T=T_t-T_b \tag{22}$$

In Eq. 20, it is assumed that the material at the bottom surface of the structure ($z=0$) is purely metallic; therefore, the metal temperature is set as $T_m=T_b$. For a layered sandwich structure consisting of **s** layers, the procedure for determining the temperature distribution along the thickness is outlined in Algorithm 1. It should be noted that the $T_t^(i-1)$ is equal to the temperature of $(i-1)^{th}$ layer at $z=h_{i-1}$.

Algorithm 1 Temperature variation along the thickness of a layered structure with **s** layers.

Require: Number of layers **s**, total thickness h, bottom temperature T_b, top temperature T_t
Ensure: Temperature distribution $T(z)$

```
for i = 1 to s do
    if i = 1 then
        T_b^(1) ← T_b
        T_t^(1) ← T_t
        Define thickness range: 0 ≤ z < h_1
    else
        T_b^(i) ← T_t^(i−1)
        T_t^(i) ← T_t
        Define thickness range: h_{i−1} ≤ z < h_i
    end if
    Compute T(z) using Eq. (20)
end for
```

4. Coordinate transformation

The complexity of the geometry (doubly-curved) presents a challenge in solving the Initial Boundary Value Problem (IBVP). This complexity can be simplified by transforming the coordinates in two steps: first, from a doubly-curved coordinate system to a single-curved one, and then from a single-curved system to a straight parallelepiped domain. This process is illustrated in Figure 2 as the master element mapping approach.

The transformation employs a simple rotational transformation approach as follows:

$$\begin{Bmatrix} x \\ y \\ z \end{Bmatrix} = \begin{bmatrix} \cos(\theta_1) & 0 & -\sin(\theta_1) \\ 0 & 1 & 0 \\ \sin(\theta_1) & 0 & \cos(\theta_1) \end{bmatrix} \begin{Bmatrix} x' - R_1\left[1-\cos(\theta_1)\right] \\ y' \\ z' - \left[z_c - R_1\sin(\theta_1)\right] \end{Bmatrix} \tag{23}$$

$$\begin{Bmatrix} x' \\ y' \\ z' \end{Bmatrix} = \begin{bmatrix} 1 & 0 & 0 \\ 0 & \cos(\theta_2) & -\sin(\theta_2) \\ 0 & \sin(\theta_2) & \cos(\theta_2) \end{bmatrix} \begin{Bmatrix} x'' - R\left[1-\cos(\theta)\right] \\ y'' \\ z'' - \left[z' - R\sin(\theta)\right] \end{Bmatrix} \tag{24}$$

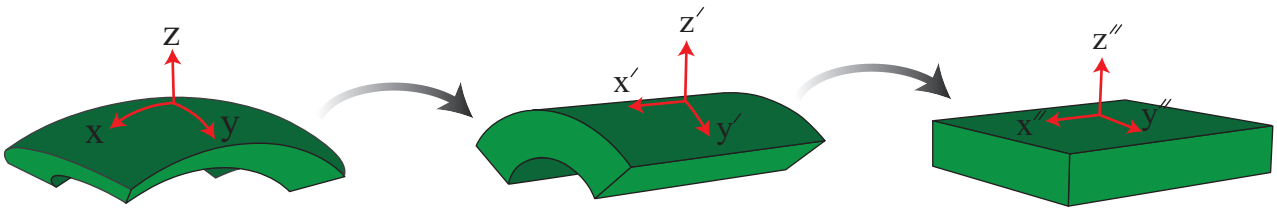

Figure 2: The transformation process from a doubly curved domain to a parallelepiped domain.

where θ_1 and θ_2 are the rotational angles around the y and x axes, respectively, associated with the curvature amount (β_i), given by:

$$\theta_i = \frac{2\pi\beta_i}{L} \tag{25}$$

From Eq. 25, the radius of curvature can be calculated as:

$$R_i = \frac{L}{2\pi\beta_i} \tag{26}$$

Thus, from the transformation equations, the Jacobian matrix can be obtained to facilitate the transformation of the problem domain from $x^{''} - y^{''} - z^{''}$ to $x - y - z$ as:

$$dxdydz = \mathbb{J}dx^{''}dy^{''}dz^{''} \tag{27}$$

5. Numerical solution: 3-D spectral Chebyshev

The three-dimensional deformation of an FGM structure can be represented as a series expansion using Tchebychev polynomials:

$$q(\xi,\eta,\zeta) = \sum_{l=1}^{\infty}\sum_{m=1}^{\infty}\sum_{n=1}^{\infty} \mathbf{a}_i \Phi_{l-1}(\xi)\Phi_{m-1}(\eta)\Phi_{n-1}(\zeta). \tag{28}$$

Here, Φ's denote orthogonal Tchebychev polynomials, and the coefficients $\mathbf{a}$ decay exponentially as i increases. It should be noted that ξ, η and ζ represent the $x^{''} - y^{''} - z^{''}$ directions, respectively. For computational purposes, the continuous function must be discretized, limiting the expansion to a finite number of terms. This is achieved using Gauss-Lobatto sampling, resulting in a third-rank tensor representation of the function:

$$q_{lmn} = q(\xi(l), \eta(m), \zeta(n)). \tag{29}$$

The indices l, m, n vary from 1 to the corresponding polynomial orders N_ξ, N_η, N_ζ along each axis. To facilitate numerical manipulation, this tensor is converted into a vector using the transformation:

$$q_i = f_{lmn}\,, \quad i = (l-1)N_\eta N_\zeta + (m-1)N_\zeta + n. \tag{30}$$

This transformation enables the sampled deflection function $\mathbf{q}$ to be linked with the expansion coefficients $\mathbf{a}$ via extended transformation matrices for forward ($\mathbf{\Gamma_F}$) and backward ($\mathbf{\Gamma_B}$) operations:

$$\mathbf{q} = \mathbf{\Gamma_B}\mathbf{a}\,, \quad \text{or} \quad \mathbf{a} = \mathbf{\Gamma_F}\mathbf{q}. \tag{31}$$

These transformation matrices, each of size $N_\xi N_\eta N_\zeta \times N_\xi N_\eta N_\zeta$, are constructed using direction-specific forward and backward matrices. Once the domain is discretized, to determine spatial derivatives, differential matrices $\mathbf{Q_{q_i}}$ are required. The derivative operation in each direction is introduced as:

$$\mathbf{b} = \mathbf{D}^{q_i}\mathbf{a}. \tag{32}$$

Using a similar mapping strategy as with the transformation matrices, the extended derivative matrices $\mathbb{D}^{\mathbf{q_i}}$ are formulated. The corresponding differential matrices are then defined as:

$$\frac{\partial \mathbf{q}}{\partial q_i} = \mathbf{Q_{q_i}}\,\mathbf{q}. \tag{33}$$

Same as the deferential matrices, the integral matrices in each direction can be determined as v_i. Therefore, by using mapping strategy and inner product approach the integral operator over the volume can be achieved ($\mathbb{V}$). Consequently, The volume integrals are evaluated using a weighted inner product matrix approach:

$$\int_{\mathbb{V}} fgAB\, d\mathbb{V} = \mathbf{f}^{\mathrm{T}}\, \mathbb{V}_{A,B}\, \mathbf{g}. \tag{34}$$

Since the integral contains functions with different weightings such as material and temperature variation along the thickness, each function must be extrapolated to an increased number of sampling points using extrapolation matrices $S^{q_{i_n}}$. This process follows:

$$\mathbf{f}_{4N_x\, 4N_y\, 4N_z} = \mathbf{S}^{x_4}\mathbf{S}^{y_4}\mathbf{S}^{z_4}\, f_{N_x\, N_y\, N_z}. \tag{35}$$

Finally, the system matrices for an unconstrained lamina can be expressed as:

$$\mathbf{M} = \begin{bmatrix} \mathbb{I}_U & \mathbb{O} & \mathbb{O} \\ \mathbb{O} & \mathbb{I}_V & \mathbb{O} \\ \mathbb{O} & \mathbb{O} & \mathbb{I}_W \end{bmatrix}^{\mathrm{T}} \begin{bmatrix} \mathbb{V}_{(\Upsilon,\mathbf{J})} & \mathbb{O} & \mathbb{O} \\ \mathbb{O} & \mathbb{V}_{(\Upsilon,\mathbf{J})} & \mathbb{O} \\ \mathbb{O} & \mathbb{O} & \mathbb{V}_{(\Upsilon,\mathbf{J})} \end{bmatrix} \begin{bmatrix} \mathbb{I}_U & \mathbb{O} & \mathbb{O} \\ \mathbb{O} & \mathbb{I}_V & \mathbb{O} \\ \mathbb{O} & \mathbb{O} & \mathbb{I}_W \end{bmatrix} \tag{36}$$

$$\mathbf{K}_e = \begin{bmatrix} Q_x & \mathbb{O} & \mathbb{O} \\ \mathbb{O} & Q_y & \mathbb{O} \\ \mathbb{O} & \mathbb{O} & Q_z \\ Q_z & \mathbb{O} & Q_x \\ Q_y & Q_x & \mathbb{O} \\ \mathbb{O} & Q_z & Q_y \end{bmatrix}^{\mathrm{T}} \begin{bmatrix} \mathbb{V}_{(\mu,\mathbf{J})} & \mathbb{V}_{(\lambda,\mathbf{J})} & \mathbb{V}_{(\lambda,\mathbf{J})} & 0 & 0 & 0 \\ \mathbb{V}_{(\lambda,\mathbf{J})} & \mathbb{V}_{(\mu,\mathbf{J})} & \mathbb{V}_{(\lambda,\mathbf{J})} & 0 & 0 & 0 \\ \mathbb{V}_{(\lambda,\mathbf{J})} & \mathbb{V}_{(\lambda,\mathbf{J})} & \mathbb{V}_{(\mu,\mathbf{J})} & 0 & 0 & 0 \\ 0 & 0 & 0 & \mathbb{V}_{(\mu,\mathbf{J})} & 0 & 0 \\ 0 & 0 & 0 & 0 & \mathbb{V}_{(\mu,\mathbf{J})} & 0 \\ 0 & 0 & 0 & 0 & 0 & \mathbb{V}_{(\mu,\mathbf{J})} \end{bmatrix} \begin{bmatrix} Q_x & \mathbb{O} & \mathbb{O} \\ \mathbb{O} & Q_y & \mathbb{O} \\ \mathbb{O} & \mathbb{O} & Q_z \\ Q_z & \mathbb{O} & Q_x \\ Q_y & Q_x & \mathbb{O} \\ \mathbb{O} & Q_z & Q_y \end{bmatrix} \tag{37}$$

$$\mathbf{K}_T = \begin{bmatrix} \mathbb{O} & \mathbb{O} \\ \mathbb{O} & \mathbb{O} \\ Q_x & Q_y \end{bmatrix} \begin{bmatrix} -\mathbb{V}_{(\mu,\mathbf{J},\Delta T)} & 0 \\ 0 & -\mathbb{V}_{(\mu,\mathbf{J},\Delta T)} \end{bmatrix} \begin{bmatrix} \mathbb{O} & \mathbb{O} & Q_x \\ \mathbb{O} & \mathbb{O} & Q_y \end{bmatrix} \tag{38}$$

where $\mathbb{I}_{\mathbf{q}_i}$ extracts the displacement components (u, v, w) from $\mathbf{q}$, e.g. $\mathbb{I}_u = [\mathbb{I}\ \mathbb{O}\ \mathbb{O}]$. The mapping algorithm is applied again to transform the weighted inner product tensor into a matrix form, completing the numerical formulation for FGM structures.

5.1. Boundary Conditions and coupling of the layers

In this section, two main issues are pursued: (i) imposing boundary conditions and (ii) coupling the layers. It should be noted that by using the IBVP approach, the natural boundary conditions are incorporated into the system matrices, while the essential boundary conditions must be explicitly imposed. Therefore, the boundary conditions can be defined in a matrix form as follows:

$$\boldsymbol{\beta}\mathbf{q}_G = \mathbf{0} \tag{39}$$

where $\mathbf{q}_G$ represents the generalized coordinates of the structure. Additionally, the coupling process can be incorporated into Eq. 39 using the compatibility equations. These equations are established by equating the degrees of freedom of the interacting surfaces of each layer. Consequently, by employing the projection matrices approach, the left singular values ($\mathbf{P}$) of the unitary matrix (v), obtained through the singular decomposition of $\boldsymbol{\beta}$, can be used to derive the resultant system matrices as follows:

$$\mathbb{M} = \mathbf{P}^{\mathrm{T}} \begin{bmatrix} \mathbf{M_1} & \mathbb{0} & \mathbb{0} \\ \mathbb{0} & \mathbf{M_2} & \mathbb{0} \\ \mathbb{0} & \mathbb{0} & \mathbf{M_3} \end{bmatrix} \mathbf{P} \tag{40}$$

$$\mathbb{K}_e = \mathbf{P}^{\mathrm{T}} \begin{bmatrix} \mathbf{K_{e_1}} & \mathbb{0} & \mathbb{0} \\ \mathbb{0} & \mathbf{K_{e_2}} & \mathbb{0} \\ \mathbb{0} & \mathbb{0} & \mathbf{K_{e_3}} \end{bmatrix} \mathbf{P} \tag{41}$$

$$\mathbb{K}_T = \mathbf{P}^{\mathrm{T}} \begin{bmatrix} \mathbf{K_{T_1}} & \mathbb{0} & \mathbb{0} \\ \mathbb{0} & \mathbf{K_{T_2}} & \mathbb{0} \\ \mathbb{0} & \mathbb{0} & \mathbf{K_{T_3}} \end{bmatrix} \mathbf{P} \tag{42}$$

where $\mathbf{M_i}$, $\mathbf{K_{e_i}}$ and $\mathbf{K_{T_i}}$ are the mass and stiffness matrices of each individual (i^{th}) lamina, calculated using Eqs. (36), (37) and (38) respectively. For more details, the reader is referred to [65, 66].

6. Convergence analysis

To obtain the converged number of polynomials, a convergence analysis is carried out. For this purpose, the reference number of polynomials is set as $N_x^{\text{ref}} = N_y^{\text{ref}} = 23$ and $N_z^{\text{ref}} = 17$. The number of polynomials is defined in the range of $[5-15]$, $[5-15]$, and $[3-11]$ for N_x, N_y, and N_z, respectively. The average values of the first ten nondimensional natural frequencies are obtained and compared to those calculated for the reference case. The nondimensional natural frequency can be calculated as:

$$\omega = \frac{\Omega L_y^2}{\pi^2} \sqrt{\frac{I_0}{D_0}} \tag{43}$$

where $I_0 = h\rho_{m0}$ and $D_0 = E_{m0}h^3/12(1-\nu_{m0}^2)$. Also, Ω is the dimensional natural frequency. The parameters ρ_{m0}, E_{m0}, and ν_{m0} represent the density, elasticity modulus, and Poisson's ratio of the metal at $T_0 = 300K$. The ceramic and metal material properties [63] are presented in Table 1.

For convergence analysis, the geometric parameters are set for a square layer as $L_x = L_y = 1$ and $h = 0.1$. The temperature difference between the top and bottom surfaces is $500K$, where the bottom surface temperature is $T_b = 300K$. The power value of the functionally graded material (FGM) is equal to 2. Also, the temperature variation is nonlinear. The results are presented in Table 2. This table shows the error percentage between the variation in the number of polynomials and the reference polynomials, which is calculated as:

$$\Xi\% = \frac{\sum_{i=1}^{10} (\omega_i^{ref} - \omega_i)}{\sum_{i=1}^{10} \omega_i^{ref}} \times 100 \tag{44}$$

Considering the error percentage in Table. 2, the efficient number of polynomials in the x-y-z directions are chosen as 11, 11 and 5, respectively.

7. Results

The Results section comprises two subsections. First, a validation study is conducted to verify the presented spectral Chebyshev method. Second, a parametric analysis is performed to investigate the effects of various parameters on the fundamental frequency of the sandwich structure.

Table 2: Convergence analysis to obtain the efficient number of polynomials in $x-y-z$ directions.

		N_y=5					N_y=7					N_y=9				
		N_z					N_z					N_z				
		3	5	7	9	11	3	5	7	9	11	3	5	7	9	11
N_x	5	15.34	14.23	14.23	14.23	14.23	8.75	6.55	6.54	6.54	6.54	8.23	6.12	6.11	6.11	6.11
	7	8.75	6.55	6.54	6.54	6.54	3.74	0.90	0.88	0.88	0.88	3.30	0.49	0.46	0.46	0.46
	9	8.23	6.12	6.11	6.11	6.11	3.30	0.49	0.46	0.46	0.46	2.96	0.21	0.17	0.17	0.17
	11	8.21	6.09	6.06	6.06	6.06	3.29	0.45	0.41	0.41	0.41	2.94	0.17	0.13	0.13	0.12
	13	8.21	6.08	6.04	6.04	6.04	3.28	0.44	0.40	0.39	0.39	2.94	0.16	0.11	0.11	0.10
	15	8.21	6.07	6.03	6.03	6.03	3.28	0.43	0.39	0.38	0.38	2.94	0.15	0.10	0.09	0.09
		N_y=11					N_y=13					N_y=15				
		N_z					N_z					N_z				
		3	5	7	9	11	3	5	7	9	11	3	5	7	9	11
N_x	5	8.21	6.09	6.06	6.06	6.06	8.21	6.08	6.04	6.04	6.04	8.21	6.07	6.03	6.03	6.03
	7	3.29	0.45	0.41	0.41	0.41	3.28	0.44	0.40	0.39	0.39	3.28	0.43	0.39	0.38	0.38
	9	2.94	0.17	0.13	0.13	0.12	2.94	0.16	0.11	0.11	0.10	2.94	0.15	0.10	0.09	0.09
	11	2.93	0.14	0.09	0.09	0.09	2.92	0.13	0.07	0.07	0.07	2.92	0.12	0.06	0.06	0.05
	13	2.92	0.13	0.07	0.07	0.07	2.92	0.12	0.05	0.05	0.05	2.91	0.11	0.05	0.04	0.04
	15	2.92	0.12	0.06	0.06	0.05	2.91	0.11	0.05	0.04	0.04	2.91	0.10	0.04	0.03	0.03

7.1. Validation

To evaluate the spectral Chebyshev approach for solving the IBVP equation, a validation study is conducted using results from the literature. The study considers three cases of temperature variation (uniform, linear, and nonlinear) along the thickness of the structure for a single layer.

For the uniform temperature variation case, the geometric parameters are set as $L_x = L_y = 0.2$ with a thickness ratio of $h/L_y = 0.1$. The curvature is assumed to be zero for all validation cases. Additionally, the power-law index is set to 2, and all edges ($x = 0, x = L_x, y = 0$ and $y = L_y$) are subjected to clamped boundary conditions with the definition of $u = v = w = 0$. The uniform temperature along the thickness is defined by $T_0 = 300K$ with temperature differences of $\Delta T = 0, 300$ and $500K$. Table 3 presents the first eight nondimensional natural frequencies obtained from spectral Chebyshev approach and those from the literature. The findings demonstrate that the spectral Chebyshev (ST) approach accurately predicts the natural frequencies of the FGM structure with temperature variation.

Table 3: Comparison of the first eight nondimensional natural frequencies of a FGM layer with uniform temperature variation where all the edges are clamped and geometry parameters are set to $L_x = L_y = 0.2$ and $h/L_y = 0.1$.

ΔT	Method	ω_1	$\omega_2(\omega_2)$	ω_4	ω_5	ω_6	ω_7	ω_8
0	Yang [67]	4.1062	7.8902	11.1834	12.5881	13.1867	15.4530	16.0017
	Kim [68]	4.1165	7.9696	11.2198	13.1060	13.2089	15.9471	15.9471
	Li [63]	4.1658	7.9389	11.1212	13.0973	13.2234	15.3627	15.3627
	ST	4.2025	8.0295	11.2586	13.2683	13.3961	15.7780	15.7780
300	Yang [67]	3.6636	7.2544	10.3924	11.7054	12.3175	14.4520	15.0019
	Kim [68]	3.6593	7.3098	10.4021	12.1982	12.3052	14.9090	14.9090
	Li [63]	3.7202	7.3010	10.3348	12.2256	12.3563	14.8112	14.8112
	ST	3.7589	7.3900	10.4709	12.3949	12.5276	15.0529	15.0529
500	Yang [67]	3.2357	6.6281	9.5900	10.8285	11.4350	13.4412	13.9756
	Kim [68]	3.2147	6.6561	9.5761	11.2708	11.3812	13.8346	13.8346
	Li [63]	3.2741	6.6509	9.5192	11.3126	11.4468	13.7907	13.7907
	ST	3.3246	6.7580	9.6778	11.5056	11.6424	14.0326	14.0326

Additionally, the spectral Chebyshev approach is examined for an FGM structure with different geometric parameters and power law indexes. For this purpose, ΔT is set to $300K$, and the boundary conditions are defined as fully clamped

on all edges. Three cases of temperature variation are considered in this validation study, where the thickness ratios (h/L_y) are 0.1 and 0.2, and the length ratios (L_x/L_y) are 0.5 and 1. Table 4 presents the first three natural frequencies obtained for the uniform and linear temperature fields and compares them to those reported in the literature [63]. Similarly, Table 5 presents the first seven natural frequencies obtained using the spectral Chebyshev approach and compares them to those from the literature for the case of a nonlinear temperature field. From the results, it can be concluded that the spectral Chebyshev approach can accurately predict the dynamic behavior of the FGM structure for different cases.

Table 4: Comparison of the first eight nondimensional natural frequencies for uniform and linear temperature variations with different geometric parameters.

$\frac{h}{L_y}$	$\frac{L_x}{L_y}$	n	Uniform						Linear					
			ω_1		ω_2		ω_3		ω_1		ω_2		ω_3	
			ST	Li[63]	ST	Li[63]	ST	Li[63]	ST	Li[63]	ST	Li[63]	ST	Li[63]
0.1	0.5	1	10.61	10.39	13.36	13.08	18.01	17.60	10.95	10.78	13.78	13.56	18.54	18.21
		2	9.34	9.21	11.76	11.59	15.84	15.60	9.68	9.59	12.18	12.06	16.37	16.20
		5	8.32	8.26	10.46	10.39	14.08	13.98	8.66	8.63	1.89	10.86	14.62	14.58
		10	7.87	7.82	9.90	9.83	13.32	13.24	8.22	8.23	10.33	10.34	13.87	13.89
	1	1	4.26	4.21	8.37	8.24	8.37	8.24	4.49	4.48	8.71	8.63	8.71	8.63
		2	3.76	3.72	7.39	7.30	7.39	7.30	3.99	3.99	7.72	7.68	7.72	7.68
		5	3.36	3.33	6.60	6.54	6.60	6.54	3.59	3.59	6.93	6.92	6.93	6.92
		10	3.18	3.14	6.24	6.19	6.24	6.19	3.41	3.42	6.58	6.59	6.58	6.59
0.2	0.5	1	7.56	7.30	9.37	9.06	11.46	11.15	7.75	7.51	9.61	9.32	11.66	11.39
		2	6.60	6.46	8.19	8.02	10.05	9.89	6.79	6.66	8.43	8.27	10.26	10.13
		5	5.81	5.77	7.22	7.18	8.96	8.89	6.01	5.98	7.47	7.43	9.18	9.13
		10	5.49	5.48	6.83	6.81	8.52	8.43	5.69	5.69	7.08	7.07	8.73	8.70
	1	1	3.68	3.60	6.49	6.31	6.49	6.31	3.79	3.72	6.67	6.51	6.67	6.51
		2	3.24	3.19	5.69	5.59	5.69	5.59	3.35	3.31	5.87	5.78	5.87	5.78
		5	2.88	2.86	5.04	5.01	5.04	5.01	2.99	2.98	5.22	5.20	5.22	5.20
		10	2.72	2.71	4.76	4.75	4.76	4.75	2.84	4.95	4.95	4.95	4.95	6.50

Table 5: Comparison of the first eight nondimensional natural frequencies for nonlinear temperature variation with different geometric parameters.

$\frac{h}{L_y}$	$\frac{L_x}{L_y}$	n	ω_1		ω_2		ω_3		ω_4		ω_5		ω_6	
			ST	Li[63]	ST	Li[63]	ST	Li[63]	ST	Li[63]	ST	Li[63]	ST	Li[63]
0.1	0.5	1	10.97	10.80	13.80	13.58	18.57	18.23	23.81	22.98	23.92	23.35	24.80	24.24
		2	9.70	9.61	12.20	12.08	16.40	16.22	20.90	20.40	21.06	20.75	21.87	21.57
		5	8.67	8.64	10.90	10.87	14.64	14.59	18.52	18.30	18.72	18.65	19.49	19.40
		10	8.22	8.23	10.34	10.35	13.88	13.90	17.53	17.42	17.75	17.75	18.47	18.47
	1	1	4.51	4.49	8.73	8.64	8.73	8.64	12.31	12.16	14.55	14.34	14.70	14.48
		2	4.00	4.00	7.74	7.70	7.74	7.70	10.90	10.82	12.88	12.77	13.01	12.89
		5	3.60	3.59	6.94	6.93	6.94	6.93	9.77	9.74	11.52	11.49	11.64	11.60
		10	3.41	3.42	6.59	6.60	6.59	6.60	9.27	9.28	10.93	10.94	11.04	11.06
0.2	0.5	1	7.76	7.52	9.62	9.33	11.68	11.40	12.51	12.12	14.54	14.23	15.57	15.13
		2	6.80	6.67	8.44	8.28	10.27	10.14	10.99	10.77	12.84	12.69	13.70	13.50
		5	6.02	5.99	7.48	7.44	9.18	9.13	9.74	9.69	11.48	11.44	12.28	12.21
		10	5.70	5.69	7.08	7.08	8.74	8.71	9.22	9.21	10.91	10.89	11.73	11.69
	1	1	3.80	3.73	6.68	6.51	6.68	6.51	8.77	8.49	8.77	8.49	8.99	8.75
		2	3.35	3.32	5.88	5.79	5.88	5.79	7.72	7.56	7.72	7.56	7.91	7.78
		5	2.99	2.98	5.22	5.20	5.22	5.20	6.89	6.82	6.89	6.82	7.02	6.99
		10	2.84	2.84	4.95	4.95	4.95	4.95	6.54	6.51	6.54	6.51	6.65	6.65

In another validation study, a curved functionally graded material (FGM) structure is analyzed in a non-thermal environment. For this purpose, a new FGM distribution equation is introduced in the literature [69] as:

Table 6: First four natural frequencies comparison for a single curved structure with the geometry parameters of $\theta_1 = 120$, $L_y = 2$ and $R = 1$ where, $y = 0$ edge is clamped.

	$n=0$			$n=1$			$n=5$			$n=50$		
$\Omega(Hz)$	SC	Ref [69]	FEM	SC	Ref [69]	FEM	SC	Ref [69]	FEM	SC	Ref [69]	FEM
1	61.8	61.5	61.8	60.9	61.0	61.0	60.3	61.5	60.4	59.1	61.0	59.0
2	96.3	95.9	96.3	95.2	94.7	94.9	93.4	95.9	92.6	91.1	94.7	90.8
3	151.8	151.2	151.7	149.3	151.2	151.0	147.9	151.2	149.5	145.3	151.2	145.5
4	243.7	243.0	243.6	240.3	241.7	240.5	237.2	243.0	237.7	232.4	241.7	232.0

$$V_c = \left(1 - a\left(\frac{1}{2} - \frac{z}{h}\right) + b\left(\frac{1}{2} - \frac{z}{h}\right)^c\right)^n \tag{45}$$

In the validation case study, the parameters of the equation are set as $a = 0.2$, $b = 0.8$, and $c = 3$, where n is the power index. The geometry of the structure is defined by $\theta_1 = 120°$, $L_y = 2$, and $R = 1$. The edge at $y = 0$ is clamped, while all other edges are free. The first four natural frequencies (in Hz) are computed using the proposed spectral Chebyshev (SC) method and compared with results reported in the literature as well as those obtained from a finite element method (FEM) analysis conducted in COMSOL software.

It is worth noting that Kandasamy et al.[69] employed the first-order shear deformation theory (FSDT) in their analysis. In contrast, the FEM simulation in this study is based on a full three-dimensional model. Table 6 presents a comparison of the results obtained from the proposed SC method, the literature, and FEM. The results clearly demonstrate that the spectral Chebyshev method yields frequencies very close to those from the FEM with 3D modeling. This suggests that three-dimensional modeling is more accurate in predicting the behavior of structures with complex material distributions compared to two-dimensional approaches. To enable an efficiency comparison in this case study, the computational time required by the proposed SC and FE methods are evaluated and compared. For the FEM, the converged number of degrees of freedom (DOFs) is 5181, whereas for the SC, it is significantly reduced to 1815. Consequently, the total computation time for the SC and FE approaches is 1.5 seconds and 7 seconds, respectively, on the same system. It should be noted that the reported SC method time includes both the modeling and solving stages, whereas the FEM time accounts only for the solving stage.

7.2. Parametric study

In this section, different parametric studies are conducted to investigate the effect of various parameters on the nondimensional fundamental frequency of the sandwich FGM structure. The sandwich structure consists of three layers: the face sheets, which are FGM layers, and a core layer made entirely of metal ($SUS304$). The outer surfaces

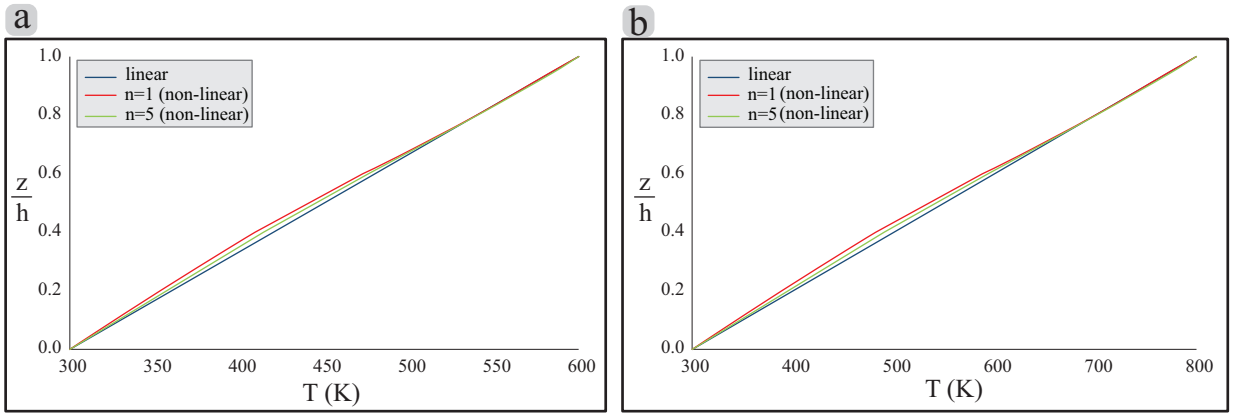

Figure 3: Temperature variation along the thickness of a sandwich structure (a) $\Delta T = 300$ and (b) $\Delta T = 500$ for linear and nonlinear temperature distributions with different power-law indices.

of the face sheets are purely ceramic (the bottom surface of the bottom layer and the top surface of the top layer), with material composition gradually varying toward the core layer. All parametric studies are performed for six temperature differences, $\Delta T = [0, 100, 200, 300, 400, 500]$.

All temperature distributions in parametric studies are assumed to follow a nonlinear variation along the thickness. However, as part of an initial parametric investigation, the effect of linear versus nonlinear temperature variation is examined. Figure 3 illustrates the temperature distribution along the thickness of the aforementioned sandwich structure for two temperature differences: (a) $\Delta T = 300$ and (b) $\Delta T = 500$. It should also be noted that the thickness ratios of the bottom, core, and upper layers are set as $h_1/h = 0.2$, $h_2/h = 0.1$, and $h_3/h = 0.2$, respectively. The results show that the temperature distributions obtained using linear and nonlinear assumptions are very similar. Therefore, it can be concluded that although solving the heat conduction equation provides a more accurate representation of the temperature variation through the thickness, assuming a linear temperature distribution offers reasonably close results with significantly reduced mathematical complexity.

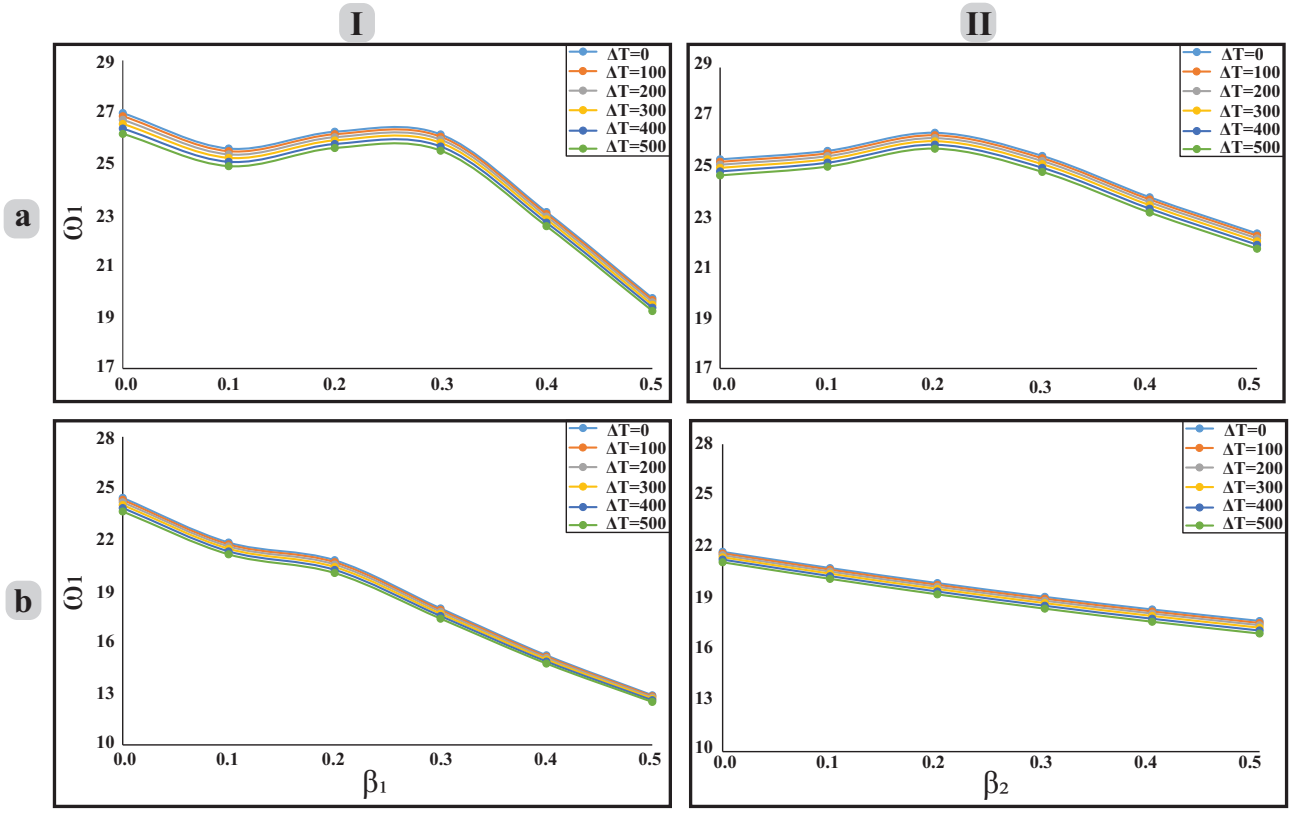

Figure 4: The effect of curvature variation on the nondimensional fundamental frequency of a sandwich FGM structure for different ΔT with imposed boundary condition of (a) $CCCC$ and (b) $FCFC$, where the face sheets are FGM layers and the core is purely metal.

To investigate the effect of geometric parameters, first, the effect of curvature on the nondimensional fundamental frequency of the sandwich structure is investigated. The geometric parameters are defined as follows: $L_x/L_y = 0.5$, $h/L_y = 0.2$, $h_1 = h_3 = h/4$, and $h_2 = h/2$. The power-law index for each face sheet is taken as 2. Figures 4 and 5 illustrate the variation in the nondimensional fundamental frequency with different curvature values under various boundary conditions. Specifically, Figures 4a and 4b present the frequency variation for $CCCC$ (all edges clamped) and $FCFC$ (clamped at $y = 0$ and $y = L$), respectively. In these figures, (I) and (II) represent the variations of the curvature parameters β_1 and β_2. For each case of curvature variation, the other curvature parameter is held constant at 0.25. The different colored lines in the plots correspond to various values of the temperature difference ΔT.

As observed in Figure 4, an increase in temperature difference (ΔT) leads to a reduction in the fundamental frequency of the sandwich FGM structure. Moreover, the frequency trend suggests that increasing the curvature reduces the overall stiffness of the structure. However, in the $CCCC$ case (Figure 4a), the fundamental frequency exhibits a local maximum around a curvature value of 0.25, which approximately coincides with the curvature value along the orthogonal axis. This suggests a possible stiffening effect when the curvatures along both directions are balanced. It

is important to note that the lengths in the x and y directions are not equal. Consequently, the dynamic behavior of the sandwich FGM structure is significantly influenced by curvature.

In continuation of the investigation on the effect of curvature on the fundamental frequency, Figures 5a and 5b present the results for $CFCF$ (clamped at $x = 0$ and $x = L$) and $CFFF$ (clamped at $y = 0$), respectively. From these figures, it can be observed that the fundamental frequency behavior differs from the trends seen in the previous boundary condition cases. In the case of β_1 variation (I), the fundamental frequency increases for both boundary conditions. It is important to note that in this scenario, the curvature and boundary constraints are applied along the shorter edge (L_x). This orientation leads to a modification of the mode shapes when compared to the $FCFC$ and $CCCC$ cases, ultimately resulting in higher fundamental frequencies.

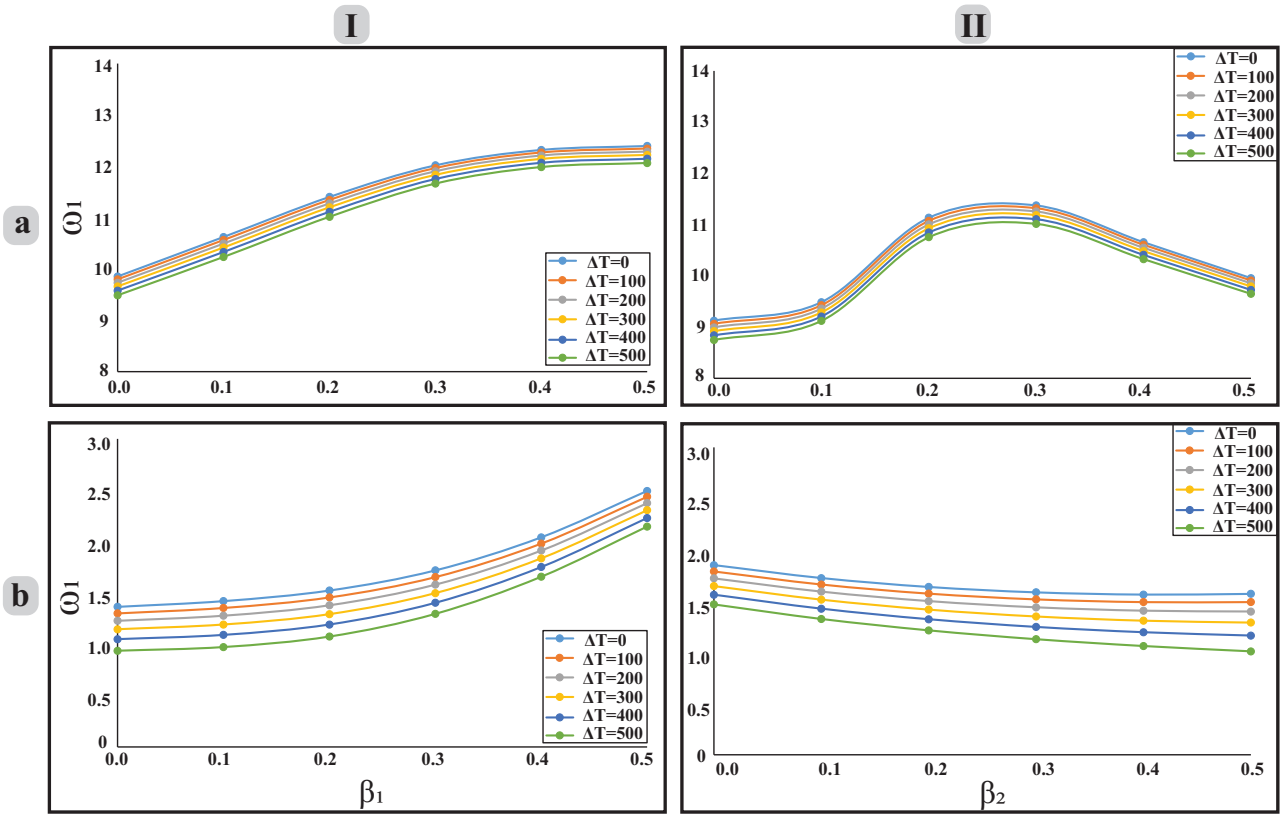

Figure 5: The effect of curvature variation on the nondimensional fundamental frequency of a sandwich FGM structure for different ΔT with imposed boundary condition of (a) $CFCF$ and (b) $CFFF$, where the face sheets are FGM layers and the core is purely metal.

The second parameter investigated in this section is the thickness ratio of the face sheets to the core layer. In this case, the ratio of the core layer thickness (h_2) to the total thickness (h) is selected as the varying parameter. The geometric parameters remain the same as in the first case study, where the initial thickness ratio is set to 0.2. Additionally, the face sheets have equal thicknesses. The curvature values are set to 0.25 for both β_1 and β_2, and the power-law index is defined as 2.

The effect of varying the thickness ratio is analyzed under different boundary conditions: $CCCC$ (all edges clamped), $FFFF$ (all edges free), $CFCF$ (clamped at x_0 and x_L, free at y_0 and y_L), and $FCFC$ (clamped at y_0 and y_L, free at x_0 and x_L). Figures 6a–d illustrate the impact of thickness ratio variation on the nondimensional fundamental frequencies for each boundary condition. Different line colors in the figures represent results for different temperature differences (ΔT).

It is evident from Figure 6 that a higher temperature difference across the thickness of the structure results in a lower fundamental frequency, implying reduced stiffness. Additionally, increasing the core layer thickness (h_2) relative to the face sheet thickness (which introduces more metallic content into the structure) leads to lower fundamental frequencies. However, in the fully free (FFFF) case, the fundamental frequency shows only slight variation with changes in thickness ratio. This behavior may be attributed to differences in the fundamental mode shapes of the structure in other case

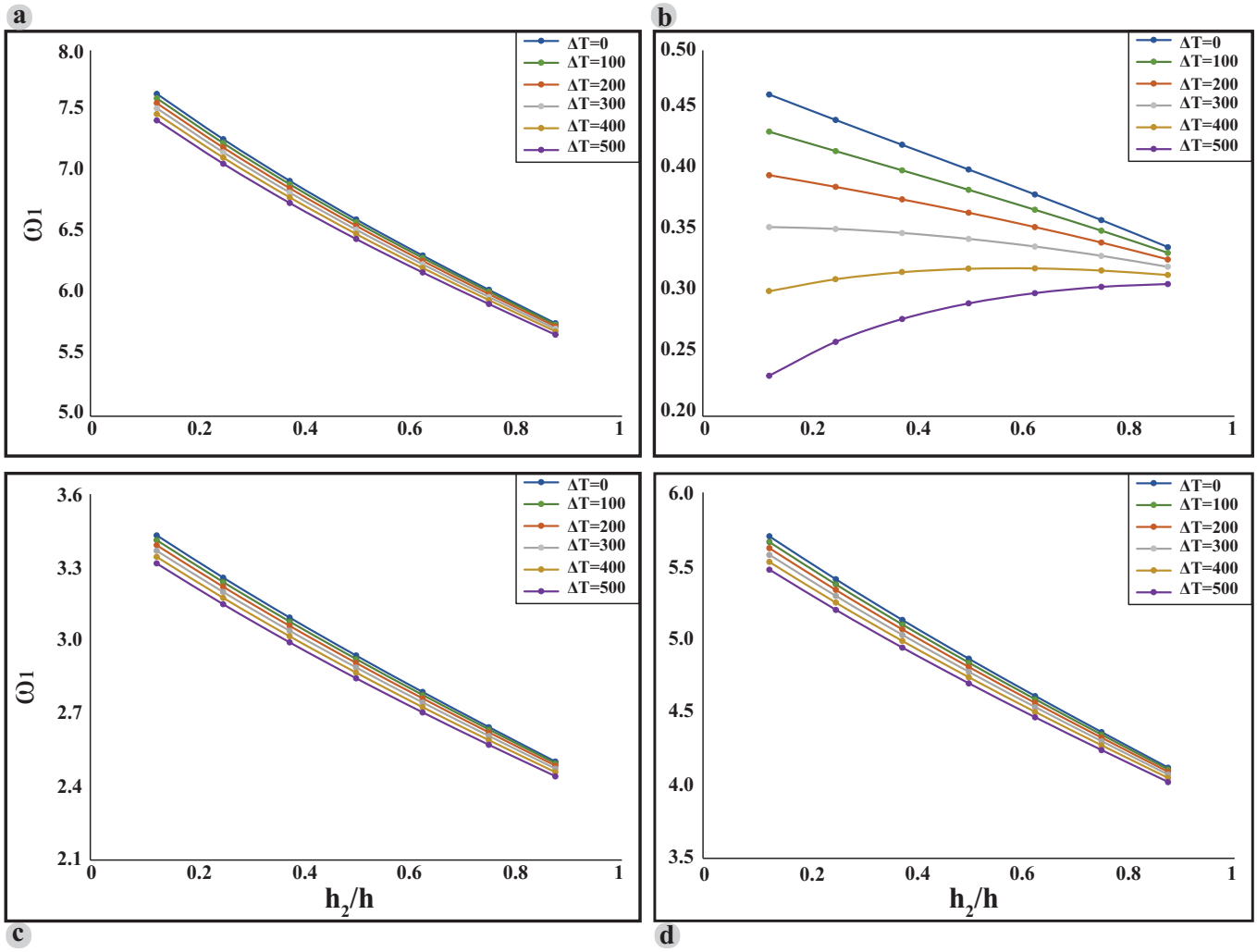

Figure 6: The effect of thickness ratio (h_2/h) on the nondimensional fundamental frequency of a sandwich FGM structure for different ΔT, where the face sheets are FGM layers and the core is purely metal.

studies. For all other boundary conditions, the center of the sandwich structure exhibits significant bending, whereas in the fully free case, the edges are more affected.

Third parameter investigated in this study is the power law index of the face sheets in the sandwich structure. In this case, the geometric parameters remain the same as in previous cases, with h_2/h set to 0.1. The effect of the power law index is examined separately for each face sheet. In other words, when n_1 (the power law index for the bottom face sheet) is the varying parameter, n_3 is fixed at 2, and when n_3 (the power law index for the top face sheet) is the varying parameter, n_1 is set to 0.2.

Figures 7a and 7b illustrate the influence of power law index variation on the fundamental frequency of the structure. Figure 7a presents the case where n_3 remains constant, while the power law index of the bottom layer (n_1) varies between 1 and 10. The results indicate that increasing the power law index of the bottom layer leads to a decrease in the fundamental frequency. In other words, a greater inclusion of the metallic phase reduces the stiffness of the structure.

Similarly, Figure 7b depicts the variation of the power law index for the top face sheet, where the power law index of the bottom face sheet is fixed at 2. In this case as well, as the face sheet incorporates more metallic content, the stiffness of the structure decreases. It is important to note that increasing the power law index results in a higher concentration of the metallic phase toward the core layer, which is composed entirely of metal. As the final parameter in the analysis, the effect of length ratio variation on the natural frequencies of the sandwich FGM structure

Table 7: The first ten natural frequencies of the sandwich FGM structure are presented for three different temperature differences and various length ratios under the $CCCC$ boundary condition.

ΔT	L_x/L_y	ω_1	ω_2	ω_3	ω_4	ω_5	ω_6	ω_7	ω_8	ω_9	ω_{10}
	1	17.31	18.18	18.45	26.46	27.92	28.41	28.73	29.49	30.75	35.46
	1.5	14.83	14.97	16.56	21.06	21.78	21.95	26.91	27.07	27.76	28.24
	2	13.87	14.06	15.94	18.14	19.08	20.18	22.72	24.63	26.10	26.55
100	2.5	13.38	13.80	15.64	17.10	17.74	19.36	20.78	22.99	23.23	26.11
	3	13.09	13.68	15.44	16.57	17.08	18.81	19.87	21.71	22.33	24.82
	3.5	12.88	13.57	15.29	16.17	16.70	18.40	19.32	21.07	21.59	24.02
	4	12.72	13.48	15.18	15.78	16.47	18.16	19.10	20.41	21.00	23.36
	1	17.14	18.00	18.27	26.21	27.63	28.11	28.46	29.17	30.46	35.12
	1.5	14.68	14.82	16.39	20.84	21.55	21.73	26.63	26.79	27.48	27.95
	2	13.73	13.92	15.78	17.95	18.88	19.97	22.48	24.39	25.83	26.29
300	2.5	13.24	13.66	15.48	16.92	17.56	19.16	20.57	22.75	23.00	25.85
	3	12.95	13.54	15.28	16.39	16.90	18.62	19.67	21.49	22.11	24.58
	3.5	12.74	13.43	15.14	16.00	16.53	18.21	19.13	20.86	21.37	23.79
	4	12.59	13.34	15.03	15.60	16.30	17.98	18.91	20.20	20.78	23.13
	1	16.93	17.78	18.05	25.89	27.27	27.75	28.10	28.77	30.08	34.69
	1.5	14.49	14.62	16.19	20.58	21.27	21.45	26.29	26.43	27.13	27.59
	2	13.55	13.74	15.58	17.73	18.64	19.72	22.19	24.07	25.49	25.94
500	2.5	13.07	13.48	15.28	16.71	17.33	18.91	20.30	22.46	22.71	25.51
	3	12.78	13.36	15.08	16.18	16.68	18.38	19.42	21.22	21.83	24.27
	3.5	12.58	13.25	14.94	15.79	16.31	17.98	18.89	20.60	21.09	23.49
	4	12.42	13.16	14.83	15.40	16.10	17.74	18.67	19.94	20.50	22.84

is investigated. Two boundary conditions are considered for this study: (i) $CCCC$ (see Table 7) and (ii) $CFFF$ (see Table 8). The parametric analysis is conducted for three different temperature differences ($\Delta T = 100$, 300, and 500). The power-law index is set to 2 for both face sheets. The thickness ratio is fixed at $h/L_y = 0.2$, with $h_1 = h_3$ and $h_1/h_2 = 0.5$.

From the results presented in both tables, it can be concluded that increasing the temperature difference leads to a decrease in all natural frequencies. This indicates that smaller temperature gradients through the thickness of the structure result in a stiffer behavior. Additionally, Table 7 shows that higher length ratios correspond to lower natural frequencies. However, a closer inspection of the data reveals a notable difference between the natural frequency values at $L_x/L_y = 1$ and those at other length ratios. This discrepancy may be attributed to a change in the mode shapes of the structure at higher length ratios.

On the other hand, the natural frequency behavior of the sandwich structure with the $CFFF$ boundary condition differs significantly from that observed in the $CCCC$ case. As shown in Table 8, the variation of the first six natural

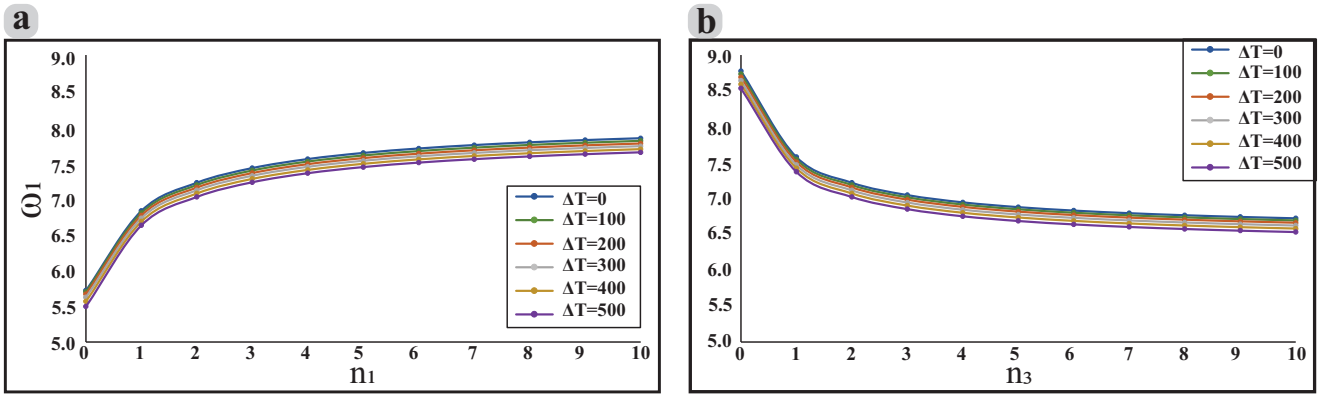

Figure 7: Effect of power law index variation of (a) bottom and (b) top face-sheets on the fundamental frequency.

Table 8: The first ten natural frequencies of the sandwich FGM structure are presented for three different temperature differences and various length ratios under the $CFFF$ boundary condition.

ΔT	L_x/L_y	ω_1	ω_2	ω_3	ω_4	ω_5	ω_6	ω_7	ω_8	ω_9	ω_{10}
	1	2.02	3.08	6.38	6.96	10.23	11.04	14.96	16.03	19.26	19.42
	1.5	2.43	3.27	6.71	7.14	8.34	10.83	12.58	15.22	15.75	16.63
	2	2.73	3.48	6.22	7.90	8.19	9.62	11.50	13.55	14.97	15.28
100	2.5	2.87	3.65	6.27	7.85	8.22	9.43	11.24	11.81	14.79	15.14
	3	2.87	3.68	6.30	7.52	8.42	9.81	10.73	11.67	14.16	14.63
	3.5	2.75	3.58	6.05	7.27	8.26	9.81	10.26	11.32	13.48	14.21
	4	2.59	3.43	5.72	7.08	7.78	8.90	9.56	9.87	10.56	12.89
	1	1.88	2.96	6.24	6.83	10.01	10.88	14.74	15.84	19.02	19.13
	1.5	2.32	3.15	6.54	7.03	8.20	10.67	12.36	15.02	15.55	16.43
	2	2.62	3.36	6.07	7.79	8.06	9.42	11.36	13.34	14.76	15.07
300	2.5	2.77	3.53	6.12	7.73	8.10	9.28	11.09	11.60	14.61	14.93
	3	2.77	3.56	6.15	7.39	8.29	9.67	10.59	11.48	13.99	14.41
	3.5	2.65	3.45	5.90	7.14	8.11	9.69	10.12	11.12	13.31	13.99
	4	2.49	3.30	3.65	5.58	6.96	7.62	9.45	9.73	10.28	12.65
	1	1.72	2.81	6.08	6.67	9.74	10.68	14.49	15.60	18.72	18.77
	1.5	2.18	3.01	6.35	6.90	8.03	10.48	12.09	14.77	15.30	16.19
	2	2.49	3.22	5.89	7.67	7.91	9.19	11.18	13.08	14.51	14.81
500	2.5	2.64	3.38	5.95	7.58	7.94	9.10	10.92	11.36	14.38	14.68
	3	2.65	3.41	5.98	7.24	8.12	9.51	10.41	11.25	13.79	14.14
	3.5	2.52	3.30	5.73	6.99	7.93	9.54	9.95	10.90	13.11	13.72
	4	2.35	3.15	5.40	6.81	7.44	9.31	9.57	10.02	11.55	12.36

frequencies exhibits a different trend compared to the higher modes. Specifically, natural frequencies from the 7^{th} to the 10^{th} mode decrease consistently with increasing length ratio. However, for the first six modes, an increase in natural frequency is observed as the length ratio increases up to $L_x/L_y = 3$, followed by a slight decrease beyond this point. This non-monotonic behavior may be attributed to mode shape transitions or shifts, commonly referred to as mode shape relocation.

8. conclusion

In this research, a novel three-dimensional spectral Chebyshev approach—developed as a meshless numerical method—is presented to investigate the dynamic behavior of doubly-curved sandwich structures reinforced with functionally graded material (FGM) face-sheets in a thermal environment. To effectively capture the geometry of the curved structure, a domain mapping technique is employed, allowing the inclusion of curvature parameters through transformation equations. The domain is discretized using Gauss-Lobatto points, which serve as efficient collocation nodes due to their compatibility with the trigonometric formulation of Chebyshev polynomials used for approximating the displacement field.

The stiffness (including initial thermal strain effects) and mass matrices are formulated individually for each layer. These are then coupled using a projection matrix to construct the global system. A steady-state thermal condition is assumed across the thickness of the structure, with a temperature gradient applied between the top and bottom surfaces. Based on Chebyshev polynomial expansions, derivative and integral operators are derived to solve the resulting integral boundary value problem (IBVP). Owing to the graded nature of the material and temperature-dependent properties along the thickness, the integral operator is treated as a weighted matrix, accurately capturing the non-uniform behavior. Convergence analysis reveals that using 11, 11, and 5 polynomials in the x, y, and z directions, respectively, yields accurate and efficient results.

To validate the proposed method, natural frequencies of single-layer FGM plates are computed and compared with existing literature for various temperature differences and length ratios. The results confirm the accuracy and reliability of the spectral Chebyshev approach in capturing the dynamic response of FGM-based structures.

Extensive parametric studies are carried out to explore the effects of boundary conditions, thermal gradients, power-law

indices, curvature, and geometric ratios on the natural frequencies of the sandwich structure. First, it is observed that increasing the temperature difference across the thickness leads to a reduction in stiffness, consequently lowering the natural frequencies. Second, the influence of curvature is found to be highly dependent on both the curvature axis and boundary conditions. For example, under fully clamped conditions or clamping along the y-edges, increasing curvature reduces the fundamental frequency at specific length ratios.

The effect of the core-to-face thickness ratio is also analyzed. It is concluded that, except in cantilever configurations, increasing the thickness of the metallic core (assumed to be a purely metallic phase of the FGM) results in a reduction in the fundamental frequency. Additionally, increasing the power-law index—where the outer face-sheet surface is purely ceramic—leads to an increase in the natural frequency due to enhanced stiffness.

Finally, the influence of varying length ratios is examined under different temperature gradients and boundary conditions. For fully clamped (CCCC) configurations, increasing the length ratio L_x/L_y consistently decreases the first ten natural frequencies. In contrast, for cantilever-type (CFFF) boundaries, a non-monotonic trend is observed: the first to sixth frequencies increase up to a critical length ratio (here, $L_x/L_y = 3$), after which they decline. The seventh to tenth frequencies, however, show a decreasing trend throughout due to mode shape shifts.

In conclusion, the proposed three-dimensional spectral Chebyshev method is shown to be an accurate and computationally efficient tool for analyzing the dynamic behavior of sandwich structures with material and geometric complexities. Moreover, the study emphasizes the sensitivity of FGM sandwich structures to geometric and thermal parameters, which must be carefully considered in the design and optimization processes for advanced composite applications.

References

[1] M. Shen, M. Bever, Gradients in polymeric materials, Journal of Materials science 7 (1972) 741–746.

[2] S. S. Vel, R. C. Batra, Three-dimensional exact solution for the vibration of functionally graded rectangular plates, Journal of Sound and Vibration 272 (3-5) (2004) 703–730. doi:10.1016/S0022-460X(03)00412-7.

[3] G. Udupa, S. S. Rao, K. Gangadharan, Functionally Graded Composite Materials: An Overview, Procedia Materials Science 5 (2014) 1291–1299. doi:10.1016/j.mspro.2014.07.442.

[4] S. Kumar Bohidar, R. Sharma, R. Mishra, Functionally Graded Materials: A Critical Review, International Journal of Scientific Footprints 2 (4) (2014) 18–29.

[5] B. Kieback, A. Neubrand, H. Riedel, Processing techniques for functionally graded materials, Materials Science and Engineering: A 362 (1-2) (2003) 81–106. doi:10.1016/S0921-5093(03)00578-1.

[6] M. M. Gasik, Functionally graded materials: bulk processing techniques, International Journal of Materials and Product Technology 39 (1-2) (2010) 20–29.

[7] M. Koizumi, Fgm activities in japan, Composites part b: engineering 28 (1-2) (1997) 1–4.

[8] W. Pompe, H. Worch, M. Epple, W. Friess, M. Gelinsky, P. Greil, U. Hempel, D. Scharnweber, K. Schulte, Functionally graded materials for biomedical applications, Materials Science and Engineering: A 362 (1-2) (2003) 40–60. doi:10.1016/S0921-5093(03)00580-X.

[9] F. Watari, A. Yokoyama, F. Saso, M. Uo, T. Kawasaki, Fabrication and properties of functionally graded dental implant, Tech. rep. (1997).

[10] Y. Li, C. Yang, H. Zhao, S. Qu, X. Li, Y. Li, New developments of ti-based alloys for biomedical applications (2014). doi:10.3390/ma7031709.

[11] K. Swaminathan, D. M. Sangeetha, Thermal analysis of FGM plates – A critical review of various modeling techniques and solution methods (1 2017). doi:10.1016/j.compstruct.2016.10.047.

[12] S. A. Sina, H. M. Navazi, H. Haddadpour, An analytical method for free vibration analysis of functionally graded beams, Materials & Design 30 (3) (2009) 741–747. doi:10.1016/J.MATDES.2008.05.015.

[13] R. Kadoli, K. Akhtar, N. Ganesan, Static analysis of functionally graded beams using higher order shear deformation theory, Applied Mathematical Modelling 32 (12) (2008) 2509–2525. doi:10.1016/J.APM.2007.09.015.

[14] A. Chakraborty, S. Gopalakrishnan, J. N. Reddy, A new beam finite element for the analysis of functionally graded materials, International Journal of Mechanical Sciences 45 (3) (2003) 519–539. doi:10.1016/S0020-7403(03)00058-4.

[15] D. K. Jha, T. Kant, R. K. Singh, A critical review of recent research on functionally graded plates (2 2013). doi:10.1016/j.compstruct.2012.09.001.

[16] K. Swaminathan, D. T. Naveenkumar, A. M. Zenkour, E. Carrera, Stress, vibration and buckling analyses of FGM plates-A state-of-the-art review (2 2015). doi:10.1016/j.compstruct.2014.09.070.

[17] Y. Chen, G. Jin, C. Zhang, T. Ye, Y. Xue, Thermal vibration of FGM beams with general boundary conditions using a higher-order shear deformation theory, Composites Part B: Engineering 153 (2018) 376–386. doi:10.1016/J.COMPOSITESB.2018.08.111.

[18] M. Talha, B. N. Singh, Static response and free vibration analysis of FGM plates using higher order shear deformation theory, Applied Mathematical Modelling 34 (12) (2010) 3991–4011. doi:10.1016/J.APM.2010.03.034.

[19] S. Çeriba, Static and Dynamic Analyses of Thin Uniformly Loaded Super Elliptical FGM Plates, Mechanics of Advanced Materials and Structures 19 (5) (2012) 323–335. doi:10.1080/15376494.2010.528160.

[20] Y. Kiani, M. R. Eslami, An exact solution for thermal buckling of annular FGM plates on an elastic medium, Composites Part B: Engineering 45 (1) (2013) 101–110. doi:10.1016/J.COMPOSITESB.2012.09.034.

[21] S. J. Singh, S. P. Harsha, Buckling analysis of FGM plates under uniform, linear and non-linear in-plane loading, Journal of Mechanical Science and Technology 33 (4) (2019) 1761–1767. doi:10.1007/S12206-019-0328-8/METRICS.

[22] H. S. Yang, C. Y. Dong, X. C. Qin, Y. H. Wu, Vibration and buckling analyses of FGM plates with multiple internal defects using XIGA-PHT and FCM under thermal and mechanical loads, Applied Mathematical Modelling 78 (2020) 433–481. doi:10.1016/J.APM.2019.10.011.

[23] M. Javani, Y. Kiani, M. Sadighi, M. R. Eslami, Nonlinear Vibration Behavior of Rapidly Heated Temperature-Dependent FGM Shallow Spherical Shells, https://doi.org/10.2514/1.J058240 57 (9) (2019) 4071–4084. doi:10.2514/1.J058240.

[24] P. L. Motlagh, M. R. Anamagh, B. Bediz, I. Basdogan, Electromechanical analysis of functionally graded panels with surface-integrated piezo-patches for optimal energy harvesting, Composite Structures 263 (2021) 113714. doi:10.1016/J.COMPSTRUCT.2021.113714.

[25] H. S. Shen, Postbuckling of FGM plates with piezoelectric actuators under thermo-electro-mechanical loadings, International Journal of Solids and Structures 42 (23) (2005) 6101–6121. doi:10.1016/J.IJSOLSTR.2005.03.042.

[26] J. Yang, S. Kitipornchai, K. M. Liew, Large amplitude vibration of thermo-electro-mechanically stressed FGM laminated plates, Computer Methods in Applied Mechanics and Engineering 192 (35-36) (2003) 3861–3885. doi:10.1016/S0045-7825(03)00387-6.

[27] P. Kumar, S. P. Harsha, Vibration response analysis of sigmoidal functionally graded piezoelectric (FGP) porous plate under thermo-electric environment, Mechanics Based Design of Structures and Machines 51 (8) (2023) 4604–4634. doi:10.1080/15397734.2021.1971090.

[28] H. Parandvar, M. Farid, Large amplitude vibration of FGM plates in thermal environment subjected to simultaneously static pressure and harmonic force using multimodal FEM, Composite Structures 141 (2016) 163–171. doi:10.1016/J.COMPSTRUCT.2016.01.044.

[29] M. M. Alinia, S. A. Ghannadpour, Nonlinear analysis of pressure loaded FGM plates, Composite Structures 88 (3) (2009) 354–359. doi:10.1016/J.COMPSTRUCT.2008.04.013.

[30] R. S. Khabbaz, B. D. Manshadi, A. Abedian, Nonlinear analysis of FGM plates under pressure loads using the higher-order shear deformation theories, Composite Structures 89 (3) (2009) 333–344. doi:10.1016/J.COMPSTRUCT.2008.06.009.

[31] M. Bateni, Y. Kiani, M. R. Eslami, A comprehensive study on stability of FGM plates, International Journal of Mechanical Sciences 75 (2013) 134–144. doi:10.1016/J.IJMECSCI.2013.05.014.

[32] J. Yang, K. M. Liew, S. Kitipornchai, Dynamic stability of laminated FGM plates based on higher-order shear deformation theory, Computational Mechanics 33 (4) (2004) 305–315. doi:10.1007/S00466-003-0533-1/METRICS.

[33] S. C. Han, W. T. Park, W. Y. Jung, A four-variable refined plate theory for dynamic stability analysis of S-FGM plates based on physical neutral surface, Composite Structures 131 (2015) 1081–1089. doi:10.1016/J.COMPSTRUCT.2015.06.025.

[34] K. M. Liew, J. Yang, S. Kitipornchai, Thermal Post-Buckling of Laminated Plates Comprising Functionally Graded Materials With Temperature-Dependent Properties, Journal of Applied Mechanics 71 (6) (2004) 839–850. doi:10.1115/1.1795220.

[35] V. R. Kar, T. R. Mahapatra, S. K. Panda, Effect of different temperature load on thermal postbuckling behaviour of functionally graded shallow curved shell panels, Composite Structures 160 (2017) 1236–1247. doi:10.1016/J.COMPSTRUCT.2016.10.125.

[36] M. Mirzaei, Y. Kiani, Thermal buckling of temperature dependent FG-CNT reinforced composite plates, Meccanica 51 (9) (2016) 2185–2201. doi:10.1007/S11012-015-0348-0/FIGURES/2.

[37] M. Şimşek, Fundamental frequency analysis of functionally graded beams by using different higher-order beam theories, Nuclear Engineering and Design 240 (4) (2010) 697–705. doi:10.1016/J.NUCENGDES.2009.12.013.

[38] Z. Belabed, M. S. Ahmed Houari, A. Tounsi, S. R. Mahmoud, O. Anwar Bég, An efficient and simple higher order shear and normal deformation theory for functionally graded material (FGM) plates, Composites Part B: Engineering 60 (2014) 274–283. doi:10.1016/J.COMPOSITESB.2013.12.057.

[39] J. K. Nath, T. Das, Static and free vibration analysis of multilayered functionally graded shells and plates using an efficient zigzag theory, Mechanics of Advanced Materials and Structures 26 (9) (2019) 770–788. doi:10.1080/15376494.2017.1410915.

[40] F. Tornabene, N. Fantuzzi, M. Bacciocchi, Free vibrations of free-form doubly-curved shells made of functionally graded materials using higher-order equivalent single layer theories, Composites Part B: Engineering 67 (2014) 490–509. doi:10.1016/J.COMPOSITESB.2014.08.012.

[41] F. Ebrahimi, A. Jafari, A Higher-Order Thermomechanical Vibration Analysis of Temperature-Dependent FGM Beams with Porosities, Journal of Engineering 2016 (1) (2016) 9561504. doi:10.1155/2016/9561504.

[42] H. T. Thai, S. E. Kim, A review of theories for the modeling and analysis of functionally graded plates and shells (9 2015). doi:10.1016/j.compstruct.2015.03.010.

[43] C. P. Wu, Y. C. Liu, A review of semi-analytical numerical methods for laminated composite and multilayered functionally graded elastic/piezoelectric plates and shells (7 2016). doi:10.1016/j.compstruct.2016.03.031.

[44] V. N. Van Do, C.-H. Lee, Nonlinear analyses of fgm plates in bending by using a modified radial point interpolation mesh-free method, Applied Mathematical Modelling 57 (2018) 1–20.

[45] C. C. Hong, GDQ computation for thermal vibration of thick FGM plates by using third-order shear deformation theory, Materials Science and Engineering: B 294 (2023) 116208. doi:10.1016/J.MSEB.2022.116208.

[46] M. Javani, M. R. Eslami, Y. Kiani, Active control of thermally induced vibrations of temperature-dependent FGM circular plate with piezoelectric sensor/actuator layers, Aerospace Science and Technology 146 (2024) 108997. doi:10.1016/J.AST.2024.108997.

[47] S. Zhong, J. Zhang, G. Jin, T. Ye, X. Song, Thermal bending and vibration of FGM plates with various cutouts and complex shapes using isogeometric method, Composite Structures 260 (2021) 113518. doi:10.1016/J.COMPSTRUCT.2020.113518.

[48] L. V. Tran, A. J. Ferreira, H. Nguyen-Xuan, Isogeometric analysis of functionally graded plates using higher-order shear deformation theory, Composites Part B: Engineering 51 (2013) 368–383. doi:10.1016/J.COMPOSITESB.2013.02.045.

[49] L. Qian, R. Batra, L. Chen, Analysis of cylindrical bending thermoelastic deformations of functionally graded plates by a meshless local petrov–galerkin method, Computational Mechanics 33 (4) (2004) 263–273.

[50] A. J. Ferreira, R. C. Batra, C. M. Roque, L. F. Qian, P. A. Martins, Static analysis of functionally graded plates using third-order shear deformation theory and a meshless method, Composite Structures 69 (4) (2005) 449–457. doi:10.1016/J.COMPSTRUCT.2004.08.003.

[51] W. Wang, G. Xue, Z. Teng, Analysis of Free Vibration Characteristics of Porous FGM Circular Plates in a Temperature Field, Journal of Vibration Engineering and Technologies 10 (4) (2022) 1369–1380. doi:10.1007/S42417-022-00452-9/FIGURES/5.

[52] Civalek, A. K. Baltacıoglu, Free vibration analysis of laminated and FGM composite annular sector plates, Composites Part B: Engineering 157 (2019) 182–194. doi:10.1016/J.COMPOSITESB.2018.08.101.

[53] C. Y. Dong, Three-dimensional free vibration analysis of functionally graded annular plates using the Chebyshev–Ritz method, Materials & Design 29 (8) (2008) 1518–1525. doi:10.1016/J.MATDES.2008.03.001.

[54] T. Van Do, D. K. Nguyen, N. D. Duc, D. H. Doan, T. Q. Bui, Analysis of bi-directional functionally graded plates by fem and a new third-order shear deformation plate theory, Thin-Walled Structures 119 (2017) 687–699. doi:10.1016/j.tws.2017.07.022.

[55] S. Srividhya, P. Raghu, A. Rajagopal, J. N. Reddy, Nonlocal nonlinear analysis of functionally graded plates using third-order shear deformation theory, International Journal of Engineering Science 125 (2018) 1–22. doi:10.1016/J.IJENGSCI.2017.12.006.

[56] B. Liu, A. J. Ferreira, Y. F. Xing, A. M. Neves, Analysis of functionally graded sandwich and laminated shells using a layerwise theory and a differential quadrature finite element method, Composite Structures 136 (2016) 546–553. doi:10.1016/J.COMPSTRUCT.2015.10.044.

[57] B. Yagci, S. Filiz, L. L. Romero, O. B. Ozdoganlar, A spectral-Tchebychev technique for solving linear and nonlinear beam equations, Journal of Sound and Vibration 321 (1-2) (2009) 375–404. doi:10.1016/J.JSV.2008.09.040.

[58] D. He, H. Xu, M. Wang, T. Wang, Transmission and dissipation of vibration in a dynamic vibration absorber-roller system based on particle damping technology, Chinese Journal of Mechanical Engineering 37 (1) (2024) 108.

[59] D. He, H. Xu, Y. Wang, M. Wang, Z. Duan, N. Yang, T. Wang, Research on vertical vibration characteristics of rolling mill based on magnetorheological fluid damper absorber, Mechanical Systems and Signal Processing 224 (2025) 112203.

[60] Y. Zhai, S. Li, X. Zhang, Vibration performance of composite doubly curved shells embedded with damping layer, International Journal of Structural Stability and Dynamics (2025) 2650265.

[61] S. Thai, V. X. Nguyen, Q. X. Lieu, Bending and free vibration analyses of multi-directional functionally graded plates in thermal environment: A three-dimensional isogeometric analysis approach, Composite Structures 295 (2022) 115797.

[62] J. N. Reddy, C. D. Chin, Thermomechanical analysis of functionally graded cylinders and plates, Journal of Thermal Stresses 21 (6) (1998) 593–626. doi:10.1080/01495739808956165.

[63] Q. Li, V. P. Iu, K. P. Kou, Three-dimensional vibration analysis of functionally graded material plates in thermal environment, Journal of Sound and Vibration 324 (3-5) (2009) 733–750. doi:10.1016/J.JSV.2009.02.036.

[64] R. Javaheri, M. R. Eslami, Thermal buckling of functionally graded plates based on higher order theory, Journal of Thermal Stresses 25 (7) (2002) 603–625. doi:10.1080/01495730290074333.

[65] M. R. Anamagh, B. Bediz, Three-dimensional dynamics of functionally graded and laminated doubly-curved composite structures having arbitrary geometries and boundary conditions, Composites Part B: Engineering 172 (2019) 533–546. doi:10.1016/J.COMPOSITESB.2019.05.087.

[66] M. Rafiei Anamagh, K. Gokalp, T. A. Akyıldız, S. Alan, K. Kaya, B. Bediz, A hybrid CPU–GPU solver based on three-dimensional spectral Chebyshev technique for determining the dynamic behavior of thick sandwich panels, Engineering Analysis with Boundary Elements 147 (2023) 181–194. doi:10.1016/J.ENGANABOUND.2022.12.003.

[67] J. Yang, H. S. Shen, VIBRATION CHARACTERISTICS AND TRANSIENT RESPONSE OF SHEAR-DEFORMABLE FUNCTIONALLY GRADED PLATES IN THERMAL ENVIRONMENTS, Journal of Sound and Vibration 255 (3) (2002) 579–602. doi:10.1006/JSVI.2001.4161.

[68] Y. W. Kim, Temperature dependent vibration analysis of functionally graded rectangular plates, Journal of Sound and Vibration 284 (3-5) (2005) 531–549. doi:10.1016/J.JSV.2004.06.043.

[69] R. Kandasamy, R. Dimitri, F. Tornabene, Numerical study on the free vibration and thermal buckling behavior of moderately thick functionally graded structures in thermal environments, Composite Structures 157 (2016) 207–221.